

Investigation of physiological swelling on conductivity distribution in lower leg subcutaneous tissue by electrical impedance tomography

R. Ogawa¹, M. R. Baidillah^{1,3}, S. Akita² and M. Takei¹

1. Graduate School of Science & Eng., Dept. Mechanical Eng., Chiba University, Chiba, Japan

2. Graduate School of Medicine, Dept. Reconstructive & Aesthetic Surgery, Chiba University, Chiba, Japan

3. Send any correspondence to: mr.baidillah@chiba-u.jp

Abstract

There is a strong need for a non-invasive measurement technique that is capable of accurately identifying the physiological condition change or heterogeneity of subcutaneous adipose tissue (SAT) by localizing the abnormalities within the compartment. This paper aims to investigate the feasibility of Electrical Impedance Tomography (EIT) to assess the interstitial fluid in subcutaneous adipose tissue as an enhancement method of bioelectrical impedance spectroscopy (BIS). Here, we demonstrate the preliminary result of EIT with a wearable 16 electrodes sensor. The image-based reference EIT with fat weighted threshold method is proposed. In order to evaluate the performance of our novel method, a physiological swelling experiment is conducted, and Multi-Frequency Bioelectrical Impedance Analysis (MFBIA) is also applied as a comparison with EIT results. The experimental results showed that the proposed method was able to distinguish the physiological swelling condition and effectively to remove the unexpected background noise. Furthermore, the conductivity variation in the subcutaneous layer had a good correlation with extracellular water volume change from MFBIA data; the correlation coefficient $R^2 = 0.927$. It is concluded that the proposed method provides a significant prospect for SAT assessment.

Keywords: Subcutaneous adipose tissue assessment, Electrical Impedance Tomography, Wearable sensor, Physiological swelling, Multi-Frequency Bioelectrical Impedance Analysis

Introduction

Variation of the physiological condition of subcutaneous adipose tissue (SAT) has been diagnosed as a part of metabolic syndrome (MetS) [1], lymphedema [2], Dercum's

disease [3], and obesities [4]. Multi-Frequency Bioelectrical Impedance Analysis (MFBIA) or Bio-Electrical impedance spectroscopy (BIS) is proposed as a rapid tool for SAT assessment as it has demonstrated a significant impedance difference between healthy and abnormal SAT [2,4,5]. MFBIA uses 8 resistive electrodes that attached on the ankle and wrist through multi-frequency impedance measurements on the whole body and its portability and noninvasive characteristic makes MFBIA more attractive for routinely physiology measurement [6].

MFBIA is used based on the fact that the current flow through biological tissue is frequency-dependent [7]. At low frequency, the membrane cell acts as high impedance. It makes the current flows only at extracellular fluid. Meanwhile, at the increase of frequency, the impedance of the cell membrane is decreasing and makes the current possible to penetrate into the intracellular fluid. Several Anthropometric parameters need to be considered to relate the measured impedance with the water content at interstitial fluid, such as body weight, body height, gender, age, postures [8]. MFBIA technique assumes a human body as a single object to be measured in which only single volumes of particular compartments are measurable [9]. However, there are a number of potential limitations to MFBIA, such as: an inability to assess heterogeneity of SAT [9,10], an inability to differentiate accurately edema type and albumin accumulation location [9,10], and the performance depends on the accuracy of the controlled clinical condition [11]. These issues make a shortcoming and leads

to the modification of MFBIA to localize body segment impedance evaluation [10,12].

Our objective is, therefore, to develop the non-invasive and low-cost medical equipment using the impedance measurement with several multi-projection, i.e., using Electrical Impedance Tomography (EIT). EIT is a noninvasive medical imaging method that can show the conductivity distribution of the human body [13–15]. In EIT, the domain (e.g., bone, muscle) is excited electrically by the electrical currents injected through the electrodes, which are discretely placed along the domain boundary (e.g., skin). The exciting electric field in the domain is determined in accordance with the geometry, the boundary conditions, and the internal distribution of the electrical properties such as conductivity. The excited voltages on the electrodes can be measured, and then used for the reconstruction of the internal conductivity distribution. As the human body has been demonstrated to have different electrical properties [16], a cross-sectional view can be reconstructed with EIT to identify any abnormalities; on the subject of the early detection of lymphedema, which is the protein accumulation in subcutaneous adipose tissue. The relative value is mostly used for the image reconstruction, i.e., a homogeneous data is taken as a reference to image the difference owing to the existence of the abnormality. However, it is troublesome considering the homogeneous reference data cannot be taken in the biomedical instrumentation as they always vary over different subjects, and the human body is composed of complex properties.

This paper aims to investigate the feasibility of EIT to assess interstitial fluid in subcutaneous adipose tissue as a preliminary step in lymphedema early-detection. We measure the right lower leg to examine to what extent our EIT system with novel threshold technique has a quality to show the morphologically same image as a sample of the MRI image. A physiological swelling experiment is then carried out to scrutinize the relationship between MFBIA and our EIT system. In order to effectively focus on the varying water contents, image-based reference EIT is proposed.

Materials and methods

Image-based reference Electrical Impedance Tomography

In EIT, as typically the given domain Ω is assumed as quasi-static condition, which has a smooth boundary $\partial\Omega$ and there is no interior current source, the following equations can be employed [17]

$$\nabla \cdot (\sigma \nabla \phi) = 0 \text{ in } \Omega \quad (1)$$

$$-\sigma \nabla \phi \cdot \mathbf{n} = -J \cdot \mathbf{n} = j \text{ on } \partial\Omega \quad (2)$$

where σ , ϕ and J are the conductivity, the scalar potential, and the current density, respectively. Here, \mathbf{n} is the outward unit normal to $\partial\Omega$ and j is the magnitude of the current

density on $\partial\Omega$ derived from the injection current through the attached electrodes E_l . Where the number of electrode $l = 1, \dots, L$. The aim of EIT is to recover $\sigma \in \mathbb{R}^n$ inside the domain Ω from Neumann boundary voltage data V , and n is the number of mesh; however, due to the high ill-posedness of the inverse problem of EIT, the solution $\hat{\sigma}$ is obtained by minimizing the output least-squares concerning the actual measured voltage data V_m and the simulated voltage data $V = S\sigma$;

$$\hat{\sigma} = \underset{\sigma}{\operatorname{argmin}} \{ \|V_m(j, \phi) - S\sigma\|^2 + \lambda^2 \|R\sigma\|^2 \} \quad (3)$$

where S , λ , and R denote the sensitivity matrix, the regularization parameter, and a regularization matrix respectively. In most cases, R is the diagonal matrix with the expected conductivity σ_m , i.e., $R_{m,m} = \sigma_m^2$, and this penalty term relates to the prior information.

As the human body is very complex and has inhomogeneous electrical properties, there are problems not only to refer a homogeneous reference conductivity but also obtaining the prior conductivity distribution. Thus, the problems can be compensated by considering the first measurement voltage data as the initial conductivity distribution and subtracting the conductivity distribution at a different time point relative to the initial conductivity. The initial conductivity distribution σ_{abs} are reconstructed using the absolute EIT method [18]. In order to observe the minuscule change of conductivity in subcutaneous tissue over the long-term standing (expressed in the subsection Experimental setup and condition), the subtraction can be performed based on the assumption that there is no distortion except for the influence from the change associated with the extracellular matrix in the subcutaneous layer. The general schematic flow of the proposed method or image-based reference EIT with fat weighted threshold method, is as follows:

Table 1. Schematic flow of image-based reference EIT.

Step 1:

Defining the filtering method to eliminate the muscle's conductivity distribution and unexpected noise background

Obtain: Equation (4)

Step 2:

Using voltage data $t = 0$ as an initial conductivity distribution, selecting the mesh of SAT on the forward problem mesh condition, calculating the fat weighted threshold value $\overline{\hat{\sigma}_{fat}} + \operatorname{std}(\hat{\sigma}_{fat})$

Obtain: the fat weighted threshold value $\overline{\hat{\sigma}_{fat}} + \operatorname{std}(\hat{\sigma}_{fat})_s$

Step 3:

Applying the filter on equation (4) to experimental data

Obtain: σ_{obs} and σ

Step 4:

Using voltage data $t = 30, 60,$ and 90 mins to evaluate the varying water content to obtain the conductivity distribution, applying equation (5)

Obtain: σ_{diff}

Considering the fact that skin is a highly resistive material and the human body has a complex conductivity distribution, we first apply the nonlinear absolute Gauss-Newton imaging [19], where we set σ_m based on reference conductivity data [16] for each body parts such that the muscle is the most conductive, which is followed by the fat and the bone in order. We choose the Laplace prior in which the regularization matrix is interpreted as a 2nd order High Pass Filter (HPF) [20]. After obtaining the inhomogeneous reference, we implement the filtering process to all the data that weights the subcutaneous layer

$$\begin{cases} \hat{\sigma}_n = \hat{\sigma}_n, & \text{if } \hat{\sigma}_n \leq \overline{\hat{\sigma}_{fat}} + std(\hat{\sigma}_{fat}) \\ \hat{\sigma}_n = \overline{\hat{\sigma}_{muscle}}, & \text{if } \hat{\sigma}_n > \overline{\hat{\sigma}_{fat}} + std(\hat{\sigma}_{fat}) \end{cases} \quad (4)$$

$\hat{\sigma}_n$ is the n th element of the estimated conductivity distribution and $\overline{\hat{\sigma}_{fat}}$ and $\overline{\hat{\sigma}_{muscle}}$ are the average of the predicted conductivity elements in the SAT layer and the muscle layer according to the FEM mesh (Figure 1), respectively. The operator $std(\cdot)$ returns the standard deviation. As for the elements which are lower than the threshold, those still entail the effect arisen from both fat and bone in light of the conductivity of bone being lower than that of fat. This FEM forward mesh is generated based on a sample of an MRI image using Netgen software (Netgen 4.9.13). Then the predicted absolute conductivity $\hat{\sigma}_{abs}$ is used as the image-based reference in the later image reconstruction as follows;

$$\hat{\sigma}_{diff} = \hat{\sigma} - \hat{\sigma}_{abs} \quad (5)$$

in which not only to reconstruct the absolute conductivity value but also to focus on the relative value. The $\hat{\sigma}_{diff}$ denotes the difference conductivity distribution compared to that of the absolute $\hat{\sigma}_{abs}$. Based on the assumption regarding the muscle and bone area, the distortion in its area is also smoothed to reduce the background noise further. Here, importantly, the image error derived from the existence of tibia, which does not accumulate liquid, could be mitigated when that influence acquired are constant

across the experiments. The advantage of this method is to be able to focus on only the abnormalities even if the background is inhomogeneous.

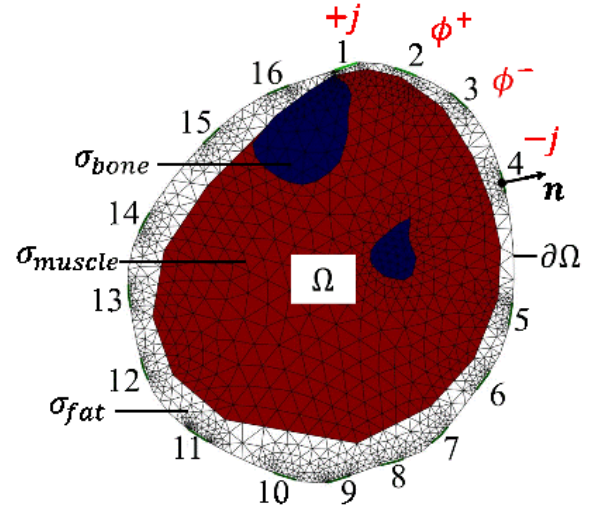


Fig. 1. The FEM forward mesh based on an MRI image. White, red, and blue part indicate SAT layer, muscle, and bone, respectively.

We implemented the quasi-adjacent stimulation and measurement pattern to accelerate the sensitivity near the boundary and the sensitivity map area [21] as the subcutaneous layer is located in the peripheral side of the domain as depicted in Figure 1.

In order to compare the quality of the proposed method, a time-difference EIT was carried out [13], where the reference was taken from the simulation data

$$\hat{\sigma}_{tdEIT} = \hat{\sigma} - \hat{\sigma}_{homo} \quad (6)$$

where $\hat{\sigma}_{homo}$ represents the homogeneous conductivity distribution. In this simulation, we assume that the lower leg has three different values, i.e., the SAT layer, muscle, and bone. Those values were as identical to those used in FEM. Other settings such as the stimulation pattern, the magnitude of current, and the frequency were the same as in the experiment.

Wearable Sensor

As the human body is not a precise circle and the shape vary significantly over the subjects, the sensor configuration is often troublesome, especially for the human subjects. We, therefore, developed a wearable EIT sensor, which has a row of 16 equidistant silver yarn electrodes and these electrodes are attached on a flexible cloth made up of polyester. The electrodes are shielded by thermoplastic polyurethane (TPU) as a countermeasure for the high contact impedance [22]. It is worth mentioning that this sensor is excellent in adhesion to the skin so that contact impedance can be reduced. Furthermore, this sensor has the capability to adapt its size and shape to any subject with less discomfort.

Experimental setup and Conditions

We used an impedance analyzer (Impedance analyzer IM3570, HIOKI) and a multiplexer (multiplexer 34970A, Agilent) as the data acquisition system, which is connected to the wearable EIT sensor and a PC using coaxial cable and USB cable, respectively, as can be seen in Figure 2. The PC has installed LabVIEW (LabVIEW 2015, National Instruments) in order to visualize the spectrum and control the data acquisition system. The amplitude of the sinusoidal current is set as 1 mA, and 1 kHz frequency is selected to focus on the extracellular fluid as the low-frequency current penetrates only in the interstitium [23,24].

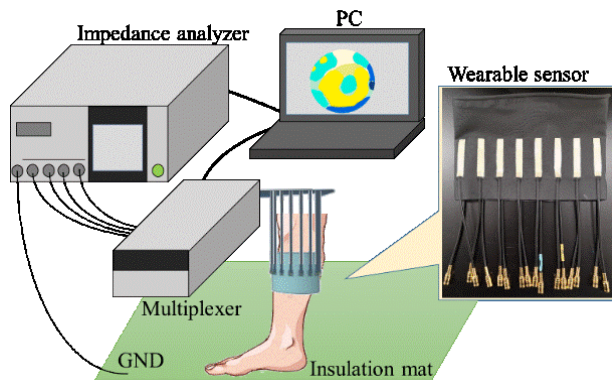


Fig. 2. Experimental setup.

A multi-frequency impedance body composition analyzer (InBodyS10, InBody Japan Inc.) was used to measure extracellular fluid volume in the right leg to acquire the varying water contents, which pertain specifically to the conductivity change.

Chester *et al.* have reported that there was change in lower leg volume over time while standing [25], therefore, in our experiments, 3 healthy male subjects (Age = 22–33 years old, BMI = 23.2–26.0) stood for 75 minutes without any minor movement except when applying the measurement devices, followed by 15-minute exercise to enhance the effect of hydrostatic pressure of the vein. EIT measurements and MFBI were taken consecutively after every 30 minutes as shown in Figure 3.

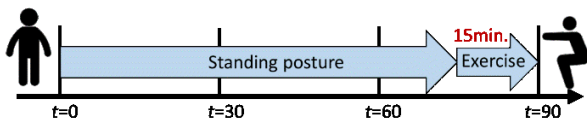


Fig. 3. Schematic diagram of the experimental schedule. After the 3rd measurement ($t = 75$ min), the subject did exercise to promote varying water contents compared to the original physiological state at the beginning of the experiment.

These experiments were carried out repeatedly for 5 days to attain the reliability of the experimental data. As MFBI data is prone to be influenced by physiological information, the subject was strictly controlled regarding life

activity such as wake-up time and breakfast menu throughout the experiment days.

Ethical approval and informed consent

Graduate School of Science and Engineering, Chiba University, Chiba, Japan, approved the study, and informed consent was obtained from the subjects. The research related to human use has been complied with all relevant national regulations, institutional policies and in accordance with the tenets of the Helsinki Declaration, and has been approved by the authors' institutional review board or equivalent committee.

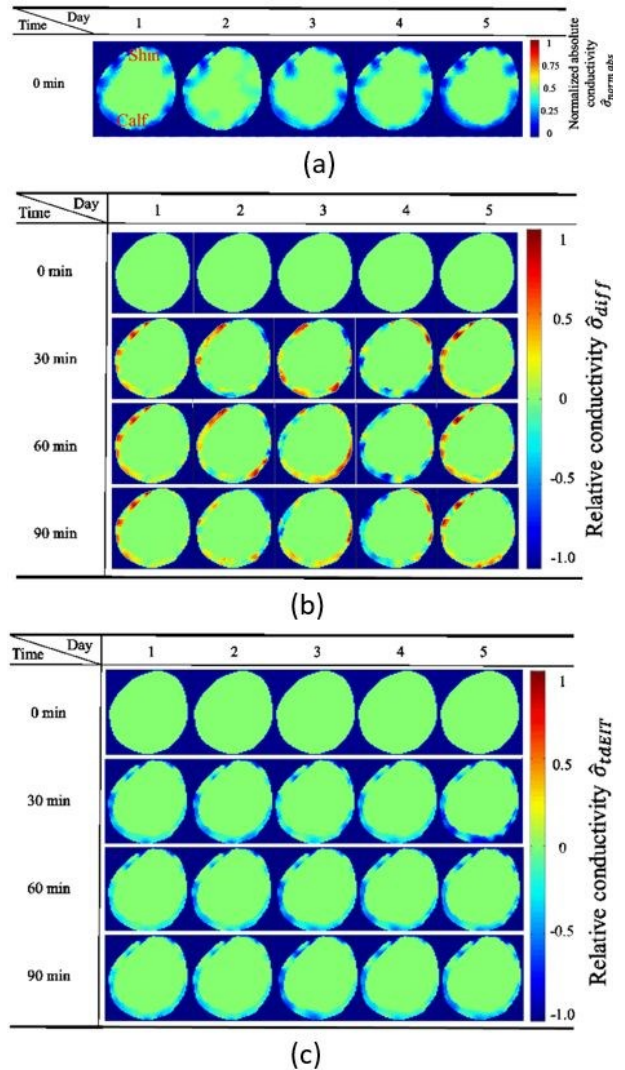


Fig. 4. (a) the normalized absolute conductivity distribution of the right lower leg (viewed from the top) reconstructed by absolute EIT at 1st measurement; These are used as inhomogeneous reference data in (b). Time series of reconstructed relative conductivity distribution using the image-based reference EIT (b) and conventional time difference EIT (c) at 2nd, 3rd, and 4th measurement, respectively.

Results

The normalized conductivity distribution reconstructed by absolute EIT on each day of one individual at the first measurement is shown in figure 4 (a), which demonstrably

showed expected results. Whereas figure 4 (b) and (c) represent the time series of the reconstructed difference conductivity distribution on each day at t = 30 mins, 60 mins, and 90 mins with the proposed method, and with the conventional time difference EIT, respectively. Figure 4 (a) reveals the predicted subcutaneous layer based on the proposed fat weighted threshold method. It has satisfactory quality with regard to the morphological relationship with an MRI image. The reconstructed SAT layer can be identified well throughout the experiment days. Although some noise can still be observed in Figure 4 (b), in which the proposed method was used, conductivity at the SAT layer is increased as time went by. This indicates water increase in the layer. On the other hand, there is almost no change in Figure 4 (c), in which the conventional time difference EIT was used; therefore, time variation cannot be observed. No change can be seen in the muscle and bone area in both methods and the impedance artefacts in the periphery arise from the influence of the measurement and the modelling errors. Similar results were acquired over the course of experiment days.

Figure 5 shows the average temporal variation of normalized segmental conductivity in the predicted subcutaneous layer (white part in Figure 1) and segmental extracellular water volume in the right leg from EIT and MFBI data, where the average of 5 days was taken at each time point. The effect of long-term standing and exercise can be seen clearly. The correlation coefficient of EIT and MFBI is achieved to $R^2 = 0.927$.

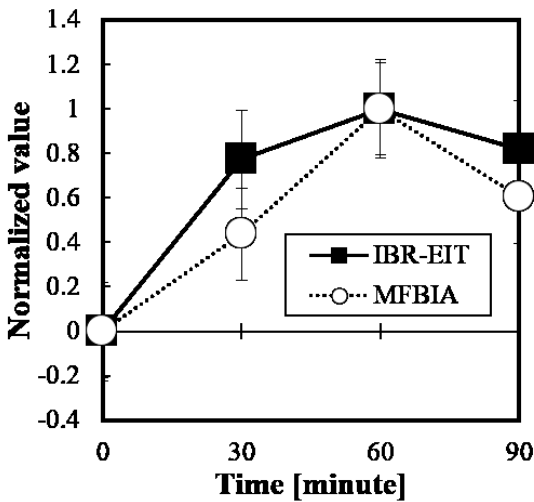


Fig. 5. The normalized temporal variation over segmental conductivity σ_{seg} in the predicted subcutaneous layer (white part in Fig.1) and segmental extracellular water volume V_{seg} in the right leg from image-based reference EIT (IBR-EIT) and MFBI data, respectively.

Discussion

The images of the SAT layer were successfully reconstructed by absolute EIT; therefore, the fat weighted threshold has a good potential to assess the interstitial fluid in the

subcutaneous adipose tissue. In fact, even though there is much background noise in the center of the images before the threshold process, this proposed method was able to reduce it sufficiently. On the other hand, as the thresholding result is calculated based on the average and the standard deviation, it may be affected when the signal-to-noise ratio (SNR) of the measurement voltage becomes lower [26]. Moreover, this thresholding can be performed based on the elements selection of the FEM mesh, hence, it highly depends on the modelling.

We realize that the MRI data used in Figure 1 is not always available for routinely monitoring by using EIT. We used one MRI data as a piece of prior known information in order to consider the inaccuracy of the reconstruction algorithm and the boundary geometry effect on the reconstructed image. Considering this prior known information, then we can obtain the average and standard deviation of SAT $\overline{\hat{\sigma}_{fat}} + std(\hat{\sigma}_{fat})$, muscle, and bone through a mesh number that is obtained from MRI. The average of the predicted conductivity of the SAT layer $\overline{\hat{\sigma}_{fat}} + std(\hat{\sigma}_{fat})$ which is a fat weighted threshold value, is used to filter the conductivity distribution of experiment data as shown in equation (4). Because the position of SAT are always near to the skin edge, obtaining the average and standard deviation of SAT $\overline{\hat{\sigma}_{fat}} + std(\hat{\sigma}_{fat})$ can use a sample from some portion of mesh that near to the wall and has lower conductivity as compared with muscle region. The most reliable approach, in order to obtain a sample from some portion of the mesh, which is close to the boundary and has low conductivity, is to define the mesh condition for the forward problem as shown in figure 1. In this mesh condition, the tibia is disregarded. This is because the image error from this tibia tends to be constant during the different time point; thus, it can be neglected in the light of the fluid analysis. The mesh of the SAT could be changed into a very thin layer in order to accommodate to a subject who is very thin.

In this study, image-based reference EIT was applied to see the variation over reconstructed conductivity distribution, where the reference was obtained using the absolute EIT at the 1st measurement to focus on the relative value as time goes by. Even though the images changed and the conductivity increased in most cases, there is a problem in the stability.

One of the reasons is the mathematical error in Equation (6). It is not enough just to subtract the value and should be compensated by introducing the penalty term or the weighted function [27]. The other reason for the lack of stability is measurement error. The subject wore the wearable sensor in the same position throughout the experiments days. It is known that even very small changes such as moisture on the skin significantly change the conductivity. Thus, these problems should be calibrated mathematically and empirically.

Conventional time difference EIT was also implemented to compare the results, where the reference was taken from the simulation data. One of the reasons why the conductivity change was too small to see the difference in the conventional time difference EIT, arises from a huge span of the magnitudes of the impedance. In the simulation, the ideal case was considered, where the electrodes were properly attached to the skin and the currents flowed through only on the two-dimensional surface. In addition to that, the contact impedance was set to a relatively small value. In the practical case, these conditions should be considered well, e.g. the electric currents are not in general confined to a two-dimensional plane [28] and the contact impedance is relatively large especially in the medical applications [29]. This same mistake about current goes for the difference of the impedance magnitude of EIT and MFBI. The former has impedance different by four orders of magnitude from that of the latter. However, it does not necessarily mean those two data sets cannot be compared as the change of the extracellular matrix due to the physiological swelling generally affects the lower leg.

Although EIT data and MFBI data had a good correlation in Figure 5, EIT images failed to sufficiently elucidate difference over time. Concerning high resistivity in the human body, especially the skin, the injected current might penetrate in an undesirable pathway. Figure 6 shows the magnitude variation of impedance at 0 min and 60 min on Day 1. Impedance decreased due to the rise in the extracellular water volume. In the quasi-adjacent stimulation, the magnitude should be the biggest at the $7 + 12 * (l - 1)$ th [16], which is when the current is injected into the sensor through electrode pair 1-2 while the boundary voltage was measured at electrode pair 9-10 in the first round. Nevertheless, measured impedance data mostly experience the periodic peak at the $12 * l$ th ($l = 1 \sim 16$) measurement pattern. By taking the morphological information into account, this is ascribed to the presence of the tibia, which is located near the skin. As bone is a high-

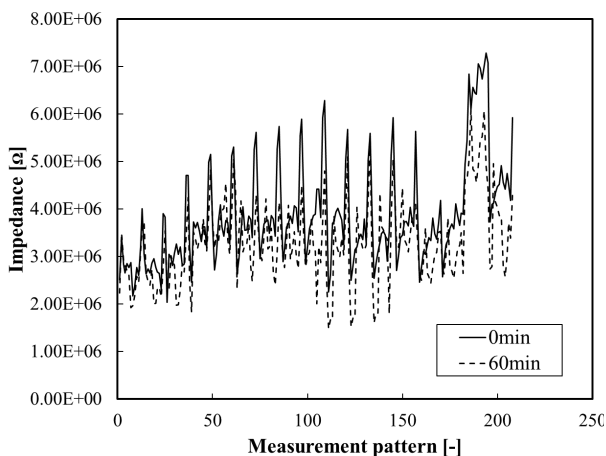


Fig. 6. The magnitude of impedance at 0 min and 60 min on Day 1.

resistive material as well as fat, and it might affect the current pathway, i.e., the accuracy of measurement data might be low when the stimulating electrodes are close to the tibia.

Conclusion

In this paper, we investigated the feasibility of our EIT system to obtain a reconstructed image, which has a good correlation with an MRI image and the MFBI data. We carried out a physiological experiment using a wearable 16 electrodes sensor and acquired the image using fat weighted threshold and image-based reference EIT. The absolute EIT images with the proposed threshold technique were able to visualize the subcutaneous adipose tissue (SAT) layer, which is morphologically similar to an MRI image of the right lower leg. Besides, the time series of EIT images have a high agreement with the MFBI data regarding varying water content of the subcutaneous fat tissues in the lower leg due to the effect of the physiological swelling over five experiment days; these achieved a correlation coefficient $R^2 = 0.927$ to the MFBI data. Although there were some errors in the images, the image-based reference EIT can focus on the distortion in the domain; furthermore, it effectively removed the unexpected background noise. It is concluded that the proposed method will be a great help to improve the treatment of lymphedema to preclude its chronic phase by applying EIT after breast cancer surgery.

Acknowledgment

This work was supported in part by the International Research Fellow of Japan Society for the Promotion of Science (Graduate School of Science and Engineering, Chiba University) and JSPS KAKENHI Grant Number JP18F18060.

Conflict of interest

Authors state no conflict of interest.

References

1. Tu AW, Humphries KH, Lear SA. Longitudinal changes in visceral and subcutaneous adipose tissue and metabolic syndrome: Results from the Multicultural Community Health Assessment Trial (M-CHAT). *Diabetes Metab Syndr Clin Res Rev.* 2017;11:S957–61. <https://doi.org/10.1016/j.dsx.2017.07.022>
2. Rockson S. Bioimpedance analysis in the assessment of lymphoedema diagnosis and management. *J Lymphoedema.* 2007;2:44–8.
3. Hansson E, Svensson H, Brorson H. Review of Dercums disease and proposal of diagnostic criteria, diagnostic methods, classification and management. *Orphanet J Rare Dis.* 2012;7:1–15. <https://doi.org/10.1186/1750-1172-7-23>
4. Yacoob Aldosky HY, Yildiz A, Hussein HA. Regional body fat distribution assessment by bioelectrical impedance analysis and its correlation with anthropometric indices. *Phys Med.* 2018;5:15–9. <https://doi.org/10.1016/j.phmed.2018.02.001>

5. Lee DH, Park KS, Ahn S, Ku EJ, Jung KY, Kim YJ, et al. Comparison of abdominal visceral adipose tissue area measured by computed tomography with that estimated by bioelectrical impedance analysis method in Korean subjects. *Nutrients*. 2015;7:10513–24. <https://doi.org/10.3390/nu7125548>
6. Lukaski HC. Evolution of bioimpedance: A circuitous journey from estimation of physiological function to assessment of body composition and a return to clinical research. *Eur J Clin Nutr*. 2013;67:S2–9. <https://doi.org/10.1038/ejcn.2012.149>
7. Ackmann JJ, Seitz MA. Methods of complex impedance measurements in biologic tissue. *Crit Rev Biomed Eng*. 1984;11:281–311.
8. Khalil SF, Mohktar MS, Ibrahim F. The theory and fundamentals of bioimpedance analysis in clinical status monitoring and diagnosis of diseases. *Sensors*. 2014;14:10895–928. <https://doi.org/10.3390/s140610895>
9. Unno N, Nishiyama M, Suzuki M, Yamamoto N, Inuzuka K, Sagara D, et al. Quantitative Lymph Imaging for Assessment of Lymph Function using Indocyanine Green Fluorescence Lymphography. *Eur J Vasc Endovasc Surg*. 2008;36:230–6. <https://doi.org/10.1016/j.ejvs.2008.04.013>
10. Rutkove SB, Aaron R, Shiffman CA. Localized bioimpedance analysis in the evaluation of neuromuscular disease. *Muscle and Nerve*. 2002;25:390–7. <https://doi.org/10.1002/mus.10048>
11. Dehghan M, Merchant AT. Is bioelectrical impedance accurate for use in large epidemiological studies? *Nutr J*. 2008;7:26. <https://doi.org/10.1186/1475-2891-7-26>
12. Scharfetter H, Monif M, László Z, Lambauer T, Hutten H, Hinghofer-Szalkay H. Effect of postural changes on the reliability of volume estimations from bioimpedance spectroscopy data. *Kidney Int*. 1997;51:1078–87. <https://doi.org/10.1038/ki.1997.150>
13. Holder DS. *Electrical Impedance Tomography: Methods, History and Applications*. CRC Press. 2004;456.
14. Adler A, Lionheart WRB. Uses and abuses of EIDORS: an extensible software base for EIT. *Physiol Meas*. 2006;27:S25–42. <https://doi.org/10.1088/0967-3334/27/5/s03>
15. Yao J, Takei M. Application of Process Tomography to Multiphase Flow Measurement in Industrial and Biomedical Fields: A Review. *IEEE Sens J*. 2017 <https://doi.org/10.1109/jsen.2017.2682929>
16. Andreuccetti D, Fossi R, Petrucci C. An Internet resource for the calculation of the dielectric properties of body tissues in the frequency range 10 Hz - 100 GHz. IFAC-CNR. 2017 [cited 2018 Oct 1]. Available from: <http://niremf.ifac.cnr.it/tissprop/>
17. Holder DS. *Electrical Impedance Tomography: Methods, History and Applications*. Holder DS, editor. CRC Press. Bristol, UK: IOP Publishing; 2005.
18. Brown BH. Electrical impedance tomography (EIT): a review. *J Med Eng Technol*. 2009;27:97–108.
19. Islam MR, Kiber MA. Electrical Impedance Tomography imaging using Gauss-Newton algorithm. 2014 Int Conf Informatics, Electron Vision, ICIEV 2014. IEEE Computer Society; 2014. <https://doi.org/10.1109/iciev.2014.6850719>
20. Sarode V, Patkar S, N Cheeran A. Comparison of 2-D Algorithms in EIT based Image Reconstruction. *Int J Comput Appl. Foundation of Computer Science*; 2013;69:6–11. <https://doi.org/10.5120/11860-7642>
21. Baidillah MR, Iman A-AS, Sun Y, Takei M. Electrical Impedance Spectro-Tomography Based on Dielectric Relaxation Model. *IEEE Sens J*. 2017;17:8251–8262. <https://doi.org/10.1109/jsen.2017.2710146>
22. Jin L, Kim KJ, Song EH, Ahn YJ, Jeong YJ, Oh TI, et al. Highly precise nanofiber web-based dry electrodes for vital signal monitoring. *RSC Adv. Royal Society of Chemistry*; 2016;6:40045–57. <https://doi.org/10.1039/c6ra00079g>
23. Ward LC, Bunce IH, Cornish BH, Mirolo BR, Thomas BJ, Jones LC. Multi-frequency bioelectrical impedance augments the diagnosis and management of lymphoedema in post-mastectomy patients. *Eur J Clin Invest*. 1992;22:751–4. <https://doi.org/10.1111/j.1365-2362.1992.tb01440.x>
24. Cornish BH, Bunce IH, Ward LC, Jones LC, Thomas BJ. Bioelectrical impedance for monitoring the efficacy of lymphoedema treatment programmes. *Breast Cancer Res Treat*. 1996;38:169–76. <https://doi.org/10.1007/bf01806671>
25. Chester MR, Rys MJ, Konz SA. Leg swelling, comfort and fatigue when sitting, standing, and sit/standing. *Int J Ind Ergon*. 2002;29:289–96. [https://doi.org/10.1016/s0169-8141\(01\)00069-5](https://doi.org/10.1016/s0169-8141(01)00069-5)
26. Yang Y, Jia J. An image reconstruction algorithm for electrical impedance tomography using adaptive group sparsity constraint. *IEEE Trans Instrum Meas*. 2017;66:2295–305. <https://doi.org/10.1109/tim.2017.2701098>
27. Jun SC, Kuen J, Lee J, Woo EJ, Holder DS, Seo JK. Frequency-difference EIT (fdEIT) using weighted difference and equivalent homogeneous admittivity: validation by simulation and tank experiment. *Physiol Meas*. 2009;30:1087–99. <https://doi.org/10.1088/0967-3334/30/10/009>
28. Rabbani KS, H.Kabir AMB. Studies on the effect of the third dimension on a two-dimensional electrical impedance tomography system. *Clin Phys Physiol Meas*. 1991;12:393–402. <https://doi.org/10.1088/0143-0815/12/4/009>
29. Rosell J, Colominas J, Riu P, Pallas-Areny R, Webster JG. Skin Impedance From 1 Hz to 1 MHz. *IEEE Trans Biomed Eng*. 1988;35:649–52. <https://doi.org/10.1109/10.4599>